JOURNAL OF GUIDANCE, CONTROL, AND DYNAMICS
Vol. 37, No. 2, March–April 2014

Orbit Radial Dynamic Analysis of Two-Craft Coulomb Formation at Libration Points

Ravi Inampudi* and Hanspeter Schaub†
University of Colorado, Boulder, Colorado 80309

DOI: 10.2514/1.55282

The linearized orbit radial dynamics and stability analysis of a two-craft virtual Coulomb structure at Earth–moon libration points are investigated. The linearized study assumes that the sunlit areas of the two-craft structure are equal such that the differential solar radiation pressure on the formation is zero. The relative distance between the two satellites of the Coulomb tether is controlled using electrostatic Coulomb forces. The separation distance between the satellites is stabilized with a charge feedback law that maintains the relative distance at a constant value. The electrostatic virtual tether between the two craft is capable of both tensile and compressive forces. The gravity gradient torques on the formation due to the two celestial objects is exploited to stabilize the Coulomb tether formation in the orbit radial direction. Controlling the separation distance stabilizes the in-plane rotation angle; however, the out-of-plane rotational motion is not affected by the spacecraft charge control law. The new two-craft dynamics at the libration points is provided as a general framework in which circular Earth orbit dynamics form a special case. Furthermore, an alternate linear control technique for a two-craft Coulomb virtual tether formation's radial equilibrium at a collinear libration point is developed and analyzed. Numerical simulations using charge feedback law are presented at both a collinear and a triangular libration point.

I. Introduction

THIS paper investigates the effectiveness of linear control techniques in stabilizing two spacecraft in a formationt virtually connected by an electrostatic (Coulomb) force moving in the presence of a restricted three-body system. This novel method of exploiting Coulomb forces for formation flying was introduced in [1,2] in 2002. Coulomb forces as a fuel efficient method for short-distance actuation in geostationary regions is discussed in [3]. Here active charge control is proposed to electrostatically inflate a large reflecting structure. The basic idea of Coulomb propulsion of free-flying vehicles is to control the spacecraft formation shape and size using the interspacecraft forces created by electrostatically charging the spacecraft to different potentials. This control is achieved by varying the charge of spacecraft by emitting either positive ions or negative electrons. For tight formation control of spacecraft separation distances on the order of 100 m or less, this propellantless thrusting is an attractive solution over conventional electric propulsion or chemical thrusting. For instance, at small separation distances between spacecraft, electric propulsion can cause thruster plume contamination of the neighboring spacecraft. However, Coulomb propulsion is a highly efficient system with a renewable energy source and I_{sp} values ranging up to 10^{13} s. Furthermore, it has very little electrical power requirements (one watt or less), and has a very high bandwidth for relative motion control with charge transition times on the order of milliseconds [1]. These advantages enable high-precision formation flying with very little fuel consumption, increasing the lifetime of the mission, and thus, the probability of mission success.

In spite of the many advantages presented by Coulomb propulsion, there are a few drawbacks. The formation dynamics are highly coupled and nonlinear; nonhomogeneous absolute spacecraft charging at geostationary altitudes may cause arcing; and dependence of the interspacecraft Coulomb forces of the whole formation on each and every spacecraft's position and charge. Furthermore, because the electrostatic forces are internal to the formation, these Coulomb forces cannot be used to control the center of mass of a nonorbiting formation. External forces such as thrusters or differential gravity gradient torques are used to reorient a Coulomb formation. Also, Coulomb formation flying requires a careful balance between the intercraft forces and the relative orbital dynamics. While Coulomb propulsion is nearly propellantless, the nonaffine nature of the charge actuation and the strongly coupled nonlinear equations of motion result in challenging and interesting control design problems.

In 2002, King et al. [1,2] introduced the Coulomb propulsion concept to control a cluster of free-flying spacecraft. Ever since their pioneering work on Coulomb formations, there have been many interesting investigations on the dynamics and control problems of Coulomb formation. King et al. [1,2] present analytic solutions for Hill-frame invariant static Coulomb formations with symmetry assumptions. The analytic open-loop solutions presented are for three- and five-craft formations, and the numerical solutions are for a six-craft formation. The charges required to maintain the formation shape are held constant and the spacecraft are placed at predefined locations in the rotating Hill frame. As a result, the Coulomb forces perfectly cancel all relative motion of the charged spacecraft, causing the static Coulomb formation to appear fixed as seen in the Hill frame. References [4–6] present more systematic analytic solutions for two-, three-, and four-spacecraft formations. Furthermore, Berryman and Schaub [6] numerically demonstrate that charged equilibria with as many as nine craft are possible in geostationary (GEO) orbits. The open-loop static Coulomb formations are all numerically unstable. Using a noncanonical Hamiltonian formulation of the Coulomb formation dynamics, Schaub et al. [7] formulate necessary conditions to achieve such static Coulomb formations with constant charges. These Hamiltonian formulations are equivalent to finding rigid body equilibrium conditions in orbit. Reference [8] applies a similar noncanonical Hamiltonian approach to examine the relative equilibria of a rigid satellite in a circular Keplerian orbit.

Natarajan [9] presents closed-loop feedback stabilized virtual Coulomb structure solutions for in-orbit two-craft configurations (radial, along-track, and orbit normal). He introduces a charge feedback law to stabilize the relative distance between the satellites exploiting the differential gravitational attraction to stabilize the attitude of a Coulomb tether formation relative to nadir. Along the

Presented as Paper 2010-7965 at the AAS/AIAA Astrodynamics Specialist Conference, Toronto, ON, Canada, 2–5 August 2010; received 14 June 2011; revision received 8 February 2012; accepted for publication 8 February 2012; published online 15 January 2014.

*Graduate Student, Aerospace Engineering Sciences Department. Member AIAA.

†Associate Professor, H. Joseph Smead Fellow, Aerospace Engineering Sciences Department. Associate Fellow AIAA.

orbit-normal and the along-track directions, the electrostatic line-of-sight actuation between two bodies and the differential gravitational accelerations are inadequate to stabilize the Coulomb tether length and the formation attitude. Therefore, to asymptotically stabilize the satellite formation shape and attitude, the authors present hybrid feedback control laws that combine conventional thrusters and Coulomb forces. Furthermore, [10] shows that for a two-spacecraft Coulomb formation at the gravitational three-body libration points, three equilibrium configurations exist (radial, along-track, and orbit normal). It's concluded that the simplified principle axes condition suffice for two-craft Coulomb tethers less than 100 m in length. Therefore, it is inferred that a second-order gravitational potential model could be used in the development of equations of motion. This paper investigates the linear dynamics and stability analysis of a two-craft Coulomb formation at Earth–moon libration points along the orbit-radial direction.

Considering a three-body system, this paper considers a two-spacecraft formation near two large masses rotating around their center of mass. For the Earth–moon system the three collinear points L_1–L_3 are unstable, while the two equilateral triangle points L_4–L_5 are stable. These equilibrium points are the libration points (L_1–L_5) in the three-body system. Tether formations at the libration points are useful for remote sensing missions to establish a long-baseline imaging capability or to ensure better stationkeeping configurations. Reference [11] considers the equilibrium configurations of a rigid tethered system near all five libration points and carries out the stability analysis when it is near the translunar libration point. Also, the report in [1] analyzes the suitability of Coulomb control for a static collinear five-vehicle formation at Earth–sun Lagrange points where the formation local dynamics ignore gravity. Reference [12] presents compatibility results of using Coulomb satellites with electric propulsion and autonomous path planning techniques at the libration points for formation keeping and reconfiguration of swarms of satellites. In the interplanetary space at a distance of 1 AU from the sun, the debye length is much smaller than that in a GEO environment (highest debye length of approximately 40 m); therefore, this constrains the maximum possible formation length, but despite the low value of the debye length, multicraft equilibrium formations are reported to exist at the Earth–sun L_1 Lagrange point [12].

These results motivate us to study the dynamics and control of a two-craft Coulomb formation at the Earth–moon libration points. To stabilize the formation shape at the libration points, a similar active charge feedback law introduced in [9] for the study of the linear dynamics of orbit radial two-craft formations at GEO is applied at the libration point scenario. The goal is to study the orbit radial dynamics and stability conditions at the libration points and to investigate the presence of any cross-coupling effects that may not exist for circular orbits at GEO. First the nonlinear and linearized equations of motion are investigated. It is of interest to compare these equations to the earlier circular GEO orbit results and to determine if these can be generalized into a single mathematical framework. To stabilize the separation distance, a partial-state charge feedback control law (separation distance and separation rate only) is studied, followed by linear stability analysis of coupled attitude and separation distance dynamics. Furthermore, an alternate linear, full-state feedback control law (in-plane attitude, separation distance, and their rates) is investigated for a radial equilibrium two-craft Coulomb tether formation at a collinear libration point. The linearized analytical results are then compared with nonlinear numerical simulations to validate the control performance results.

II. Linear Dynamics and Stability Analysis: Collinear Libration Points

A. Charged Relative Equations of Motion

The linearized equations of motion for a two-spacecraft Coulomb formation at a collinear Earth–moon libration point are briefly derived in this section. The characteristics of the frames involved in the analysis and the notation used are summarized.

Let M_1 and M_2 be the dominant masses of the two gravitational primaries, Earth and moon. As shown in Fig. 1, if O is the center of mass of both primaries, any nonrotating frame with origin at O is considered as an inertial frame. The circular relative motion of primaries occurs in a plane with angular rotation axis. The synodic frame $\mathcal{S}:\{\hat{e}_r, \hat{e}_\theta, \hat{e}_h\}$ is rotating around the O–z axis with the constant angular velocity. Ω defined as

$$\Omega = \sqrt{\frac{G(M_1 + M_2)}{d^3}} \tag{1}$$

Here G is the gravity constant and d is the distance between the two planets. The primaries are at rest in the synodic frame at positions $M_1(-d_1, 0, 0)$ and $M_2(d_2, 0, 0)$. If $\boldsymbol{r}_0 = [r_{x_0}, r_{y_0}, r_{z_0}]^T$ is the position vector in the synodic frame $\mathcal{S}$ of a collinear libration point L_2 with respect to the barycenter O, then the two distance vectors of L_2 from the two primaries in the plane are

$${}^{\mathcal{S}}\boldsymbol{R_1} = \begin{bmatrix} r_{x_0} + d_1 \\ 0 \\ 0 \end{bmatrix} \quad \text{and} \quad {}^{\mathcal{S}}\boldsymbol{R_2} = \begin{bmatrix} r_{x_0} - d_2 \\ 0 \\ 0 \end{bmatrix} \tag{2}$$

To describe the relative motion of the satellite with respect to the formation center of mass, a rotating Hill orbit frame $\mathcal{O}:\{\hat{\boldsymbol{o}}_r, \hat{\boldsymbol{o}}_\theta, \hat{\boldsymbol{o}}_h\}$ whose origin coincides with L_2 libration point is chosen as shown in Fig. 2. The formation center of mass is assumed to be at the origin of this rotating Cartesian coordinate system and the relative position vector of the ith satellite is defined as $\rho_i = (x_i, y_i, z_i)^T$; where the x_i component is in the $\hat{\boldsymbol{o}}_r$ direction (orbit radial), the y_i component is in the $\hat{\boldsymbol{o}}_\theta$ direction of orbital velocity (along-track), and the component z_i is in the $\hat{\boldsymbol{o}}_h$ direction (orbit normal). Because the orbit frame origin coincides with the formation center of mass, the center of mass condition is defined as

$$m_1\boldsymbol{\rho_1} + m_2\boldsymbol{\rho_2} = 0 \tag{3}$$

where m_i is the satellite mass. Also, for a collinear libration point, the orbit frame and the synodic frames coincide so that the position vectors $\boldsymbol{R}_1$ and $\boldsymbol{R}_2$ are equivalent in both frames.

If the two-craft formation is treated as a rigid body and aligned in the radial direction, then, for this orbit nadir aligned formation, consider a body-fixed coordinate frame $\mathcal{B}:\{\hat{\boldsymbol{b}}_1, \hat{\boldsymbol{b}}_2, \hat{\boldsymbol{b}}_3\}$ where $\hat{\boldsymbol{b}}_1$ is aligned with the relative position vector $\boldsymbol{\rho_1}$ of mass m_1. Therefore, in this configuration, the $\mathcal{O}$ and $\mathcal{B}$ frame orientation vectors are exactly aligned and $\boldsymbol{\rho_1}$ in a body-fixed frame is given by

$$\boldsymbol{\rho_1} = \frac{m_2}{m_1 + m_2} L\hat{\boldsymbol{b}}_1 + 0\hat{\boldsymbol{b}}_2 + 0\hat{\boldsymbol{b}}_3 \tag{4}$$

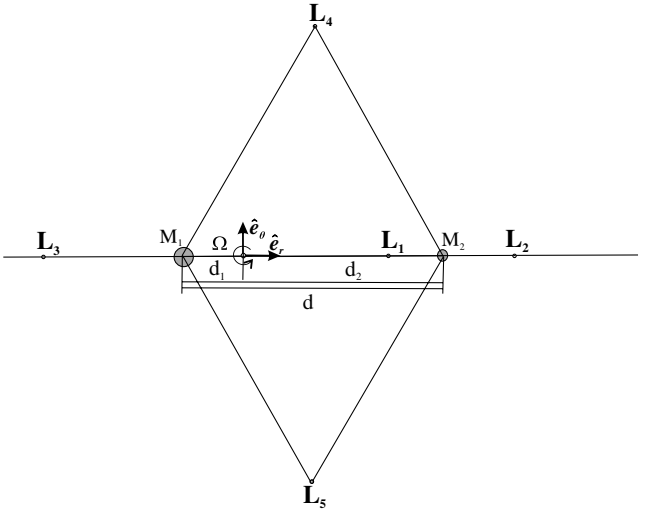

Fig. 1 Stationary libration points.

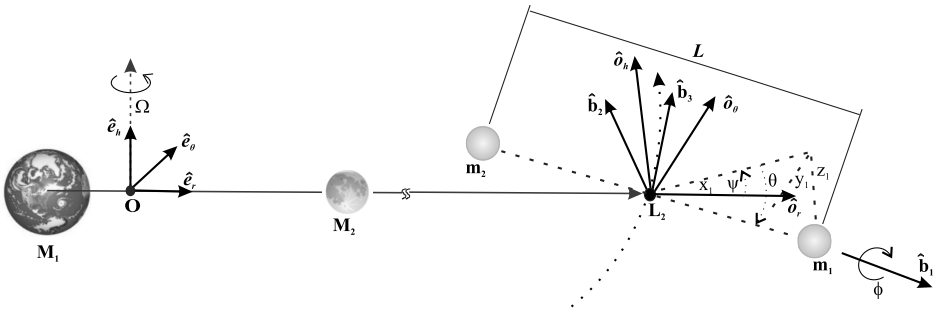

Fig. 2 Euler angles representing the attitude of Coulomb tether with respect to the orbit frame at L_2.

where L is the distance between the satellites 1 and 2. Let the 3-2-1 Euler angles (ψ, θ, ϕ) be the pitch, roll, and yaw angles that represent the relative attitude between the $\mathcal{B}$ and $\mathcal{O}$ frames. From the point-mass assumption of the two-craft, the yaw rotation about $\hat{\boldsymbol{b}}_1$ (angle ϕ) can be ignored. Then the direction cosine matrix $[BO(\psi, \theta)]$ that relates the $\mathcal{O}$ frame to $\mathcal{B}$ frame is given by

$$[BO] = \begin{bmatrix} \cos\theta\cos\psi & \cos\theta\sin\psi & -\sin\theta \\ -\sin\psi & \cos\psi & 0 \\ \sin\theta\cos\psi & \sin\theta\sin\psi & \cos\theta \end{bmatrix} \tag{5}$$

Consequently, the position vector of mass m_1 in the $\mathcal{O}$ frame is written as

$${}^{\mathcal{O}}\boldsymbol{\rho_1} = \begin{pmatrix} x_1 \\ y_1 \\ z_1 \end{pmatrix} = [BO]^T \begin{pmatrix} \frac{m_2 L}{m_1+m_2} \\ 0 \\ 0 \end{pmatrix} = \frac{m_2 L}{m_1+m_2} \begin{bmatrix} \cos\theta\cos\psi \\ \cos\theta\sin\psi \\ -\sin\theta \end{bmatrix} \tag{6}$$

Using Eq. (3), the position vector of mass m_2 in the $\mathcal{O}$ frame becomes

$${}^{\mathcal{O}}\boldsymbol{\rho_2} = \begin{pmatrix} x_2 \\ y_2 \\ z_2 \end{pmatrix} = \frac{m_1 L}{m_1+m_2} \begin{bmatrix} -\cos\theta\cos\psi \\ -\cos\theta\sin\psi \\ \sin\theta \end{bmatrix} \tag{7}$$

Furthermore, using the transport theorem [13], the inertial velocity of mass m_i expressed in the $\mathcal{O}$ frame components becomes

$${}^{\mathcal{O}}\boldsymbol{v_i} = \begin{pmatrix} \dot{x}_i - \Omega y_i \\ \dot{y}_i + \Omega(x_i + r_c) \\ \dot{z}_i \end{pmatrix} \tag{8}$$

The center of mass position vector r_c is assumed to have a constant orbital rate of Ω. The kinetic energy of the system is given by

$$T = \frac{1}{2} m_1 \boldsymbol{v_1} \cdot \boldsymbol{v_1} + \frac{1}{2} m_2 \boldsymbol{v_2} \cdot \boldsymbol{v_2} \tag{9}$$

Using Eqs. (6–8), Eq. (9) is rewritten as

$$T = \frac{1}{2}\frac{m_1 m_2}{m_1+m_2}[\dot{L}^2 + L^2(\dot{\theta}^2 + (\dot{\psi}+\Omega)^2\cos^2\theta)] + \frac{1}{2}(m_1+m_2)\Omega^2 r_c^2 \tag{10}$$

The gravitational potential energy of the two-craft formation due to the two planets is

$$V_g = -GM_1\left(\frac{m_1}{|\boldsymbol{R}_1+\boldsymbol{\rho}_1|} + \frac{m_2}{|\boldsymbol{R}_1+\boldsymbol{\rho}_2|}\right) - GM_2\left(\frac{m_1}{|\boldsymbol{R}_2+\boldsymbol{\rho}_1|} + \frac{m_2}{|\boldsymbol{R}_2+\boldsymbol{\rho}_2|}\right) \tag{11}$$

Substituting $\mu_1 = GM_1$, $\mu_2 = GM_2$, $\boldsymbol{\rho_1} = \frac{m_2}{m_1+m_2} L\boldsymbol{t_1}$, and $\boldsymbol{\rho_2} = \frac{m_1}{m_1+m_2} L\boldsymbol{t_2}$, the expression for $\frac{1}{|\boldsymbol{R}_1+\boldsymbol{\rho}_1|}$ expanded in a Taylor series about the equilibrium point, and retaining up to the second-order terms of $\frac{L}{R_1}$, becomes

$$\frac{1}{|\boldsymbol{R}_1+\boldsymbol{\rho}_1|} = \frac{1}{R_1}\left\{1 - \frac{m_2}{m_1+m_2}\left(\frac{L}{R_1}\right)\boldsymbol{u}_1\cdot\boldsymbol{t}_1 + \left(\frac{m_2}{m_1+m_2}\right)\left(\frac{L}{R_1}\right)^2(3(\boldsymbol{u}_1\cdot\boldsymbol{t}_1)^2-1)\right\} \tag{12}$$

where

$$\boldsymbol{t}_1 = \cos\theta\cos\psi\,\hat{\boldsymbol{o}}_r + \cos\theta\sin\psi\,\hat{\boldsymbol{o}}_\theta - \sin\theta\,\hat{\boldsymbol{o}}_h \tag{13}$$

$$\boldsymbol{t}_2 = -\cos\theta\cos\psi\,\hat{\boldsymbol{o}}_r - \cos\theta\sin\psi\,\hat{\boldsymbol{o}}_\theta + \sin\theta\,\hat{\boldsymbol{o}}_h \tag{14}$$

and $\boldsymbol{u}_1, \boldsymbol{u}_2$ are the unit vectors in the direction of $\boldsymbol{R}_1$ and $\boldsymbol{R}_2$.

After carrying out similar approximations for the other terms in Eq. (11), V_g finally becomes

$$V_g = -\frac{\mu_1}{R_1}\left\{(m_1+m_2) + \frac{1}{2}\frac{m_1 m_2}{(m_1+m_2)}\left(\frac{L}{R_1}\right)^2(3(\boldsymbol{u}_1\cdot\boldsymbol{t}_1)^2-1)\right\} - \frac{\mu_2}{R_2}\left\{(m_1+m_2) + \frac{1}{2}\frac{m_1 m_2}{(m_1+m_2)}\left(\frac{L}{R_2}\right)^2(3(\boldsymbol{u}_2\cdot\boldsymbol{t}_2)^2-1)\right\} \tag{15}$$

and the Coulomb potential for the two-craft formation [1] is

$$V_c = k_c\frac{q_1 q_2}{L}e^{-L/\lambda_d} \tag{16}$$

where q_i is the satellite charge and the parameter $k_c = 8.99 \times 10^9\ \mathrm{Nm^2/C^2}$ is Coulomb's constant. The exponential term in the Coulomb potential depends on the debye length parameter λ_d, which controls the electrostatic field strength of plasma shielding between the craft. At GEO the debye length varies between 80 and 1400 m, with a mean of about 180 m [14]. In the interplanetary space at Earth–moon libration points, the debye length varies between 10 and 40 m [1,15]. Note that the simple point charge electrostatic field formulation in Eq. (16) assumes that the vehicle potential is small compared with the local plasma temperature. As discussed in [16], this charge shielding formulation forms a conservative lower bound on the actual electrostatic force created between two charged bodies. For example, assuming an actual debye length of 4 m and a 1-m-diameter sphere at 30 kV yields effective debye lengths $\hat{\lambda}_d$, which are three times larger. As a result, because we are considering kilovolt levels of potential, the effective debye lengths in deep space still yield charged relative motion dynamics that are primarily influenced through classical electrostatics.

The nonlinear equations of motion are deduced from the Lagrangian $\mathcal{L} = T - (V_g + V_c)$ of the system in the following form

$$\frac{\mathrm{d}}{\mathrm{d}t}\frac{\partial\mathcal{L}}{\partial\dot{q}^i} - \frac{\partial\mathcal{L}}{\partial q^i} = \mathcal{Q}_i \quad q^i = (\theta, \psi, L) \qquad (i = 1\ldots3) \tag{17}$$

where $\mathcal{Q}_i$ is the generalized force in the q^ith degree of freedom excluding gravitational effects. For the circularly restricted three-body system, using Eqs. (10), (15), and (16) in Eq. (17), the nonlinear

equations governing the roll angle θ out of the orbital plane, the pitch angle ψ in the orbital plane, and the separation distance L become

$$\ddot{\theta} + 2\dot{\theta}\frac{\dot{L}}{L} + \cos\theta\,\sin\theta((\dot{\psi}+\Omega)^2 + 3\Omega^2\sigma\cos^2\psi) = 0 \quad (18a)$$

$$\ddot{\psi} - (\dot{\psi}+\Omega)\left(2\dot{\theta}\,\tan\theta - 2\frac{\dot{L}}{L}\right) + 3\Omega^2\sigma\,\sin\psi\,\cos\psi = 0 \quad (18b)$$

$$\ddot{L} - L(\dot{\theta}^2 + (\dot{\psi}+\Omega)^2\cos^2\theta - \Omega^2\sigma(1-3\cos^2\theta\cos^2\psi)) + \frac{k_c}{m_1}Q\frac{1}{L^2}\frac{m_1+m_2}{m_2} = 0 \quad (18c)$$

where $Q = q_1q_2$, $\nu = \dfrac{M_2}{M_1+M_2}$, $1-\nu = \dfrac{M_1}{M_1+M_2}$ and

$$\sigma = \frac{1-\nu}{\left|(r_{x_0}/d)+\nu\right|^3} + \frac{\nu}{\left|(r_{x_0}/d)-1+\nu\right|^3} > 0 \quad (19)$$

is a positive constant that depends on the collinear Lagrangian point chosen. The equations of motion [Eq. (18)] are coupled nonlinear ordinary differential equations that define the motion of a two-craft Coulomb formation at any of the three collinear Lagrangian points. If the two-craft formation is aligned in the radial direction, the formation remains statically fixed relative to the rotating orbiting frame $\mathcal{O}$ provided the nonlinear equations Eq. (18) satisfy the following radial equilibrium conditions:

$$\theta = \dot{\theta} = \ddot{\theta} = \psi = \dot{\psi} = \ddot{\psi} = \dot{L} = \ddot{L} = 0 \quad \text{and} \quad L = L_{\text{ref}} \quad (20)$$

Equation (18c) provides the nominal product of charges $Q_{\text{ref}} = q_1q_2$ needed to achieve this static Coulomb formation as

$$Q_{\text{ref}} = -(2\sigma+1)\Omega^2\frac{L^3}{k_c}\frac{m_1m_2}{m_1+m_2} \quad (21)$$

Thus, the satellites appear frozen with respect to the rotating frame when the charge product Q_{ref} satisfies Eq. (21). Because the charge product term is negative it implies that the spacecraft charges will have opposite charge signs and also, an infinite number of charge pairs can satisfy $Q_{\text{ref}} = q_1q_2$. Although unequal charges are possible between the two crafts, in this study, the charge magnitudes are set equal.

The linearized version of the nonlinear equations [Eq. (18)] are obtained by applying a Taylor series expansion about the equilibrium states given in Eq. (20). Both the roll and pitch equations of motion are linearized about small roll and pitch angles, respectively. The separation distance equations of motion are linearized about small variations in δL as well as about small variations in the product charge term δQ as follows:

$$L = L_{\text{ref}} + \delta L \quad (22a)$$

$$Q = Q_{\text{ref}} + \delta Q \quad (22b)$$

where mission requirements determine the reference separation length L_{ref}, and Q_{ref} is determined through the constraint Eq. (21) for a particular choice of L_{ref}. Performing the necessary linearizations yields

$$\ddot{\theta} + (1+3\sigma)\Omega^2\theta = 0 \quad (23a)$$

$$\ddot{\psi} + \frac{2\Omega}{L_{\text{ref}}}\delta\dot{L} + 3\sigma\Omega^2\psi = 0 \quad (23b)$$

$$\delta\ddot{L} - 2\Omega L_{\text{ref}}\dot{\psi} - 3(2\sigma+1)\Omega^2\delta L - \left(\frac{k_c}{m_1}\frac{1}{L_{\text{ref}}^2}\frac{m_1+m_2}{m_2}\right)\delta Q = 0 \quad (23c)$$

Thus, Eqs. (23a and 23b) and are the linearized attitude dynamics of the Coulomb tether body frame $\mathcal{B}$ and Eq. (23c) is the linearized separation distance differential equation about the static nadir reference configuration at a collinear libration point.

Interestingly, for $\sigma = 1$, the equations turn out to be the same equations that were found in [9] for orbit radial two-craft formation at GEO. Thus, the linearized equations of motion for small motions about orbit radial equilibria in Eqs. (23) form a general framework that covers both circular GEO and collinear libration point departure motion. By changing the constant σ either motion is described. Furthermore, in Eq. (23c) the stiffness term on δL is the only difference in the separation distance differential equation from [9]. Thus, the equations of motion are slightly different at a collinear libration point, but no significant changes in the stability behavior are expected. And, note that Eq. (23c) provides the necessary relationship between the change in relative separation of the satellites δL and the additional charge product δQ required.

It is inferred from these equations that the out-of-plane motion $\theta(t)$ is uncoupled from the in-plane motion ($\psi(t)$ and $\delta L(t)$) and is analogous to that of simple oscillatory motion because of the gravity gradient torques due to the two planets. Also, in this linearized analysis, the decoupling of the roll motion $\theta(t)$ from $\psi(t)$, $\delta L(t)$ and $\delta Q(t)$ prevents the control of roll motion using Coulomb charge. Moreover, in a special case where the satellites are at rest with no Coulomb force between them ($Q = \delta Q(t) = \dot{\psi} = 0$), Eq. (23c) simplifies to that of an unstable oscillator. Therefore, without any active Coulomb force, the two-craft formation cannot stay at the specified locations. Furthermore, $\delta L(t)$ is coupled to the body frame pitch rate $\dot{\psi}(t)$ and the pitch motion $\psi(t)$ is coupled with the $\delta L(t)$ motion, which may make it possible to control the charge for asymptotic stabilization. This coupling effect is analytically proven in the next section using the controllability properties.

B. Feedback Control Development

Under the influence of external disturbances such as solar radiation pressure, the two-craft formation deviates from the desired radial equilibrium configuration. Because the deviations from the desired equilibrium configuration are small, linear control design techniques are used to stabilize the in-plane motion without exceeding the charge requirements. In this section, two control laws are designed and compared that are used to control the in-plane motion. First, the in-plane motion is controlled with Coulomb forces using a partial-state charge feedback control defining the small charge product variation with a proportional-derivative feedback control of small separation distances. The Coulomb force acts along the relative position vector due to the charges of each craft and thus, these Coulomb charges can be used to control the spacecraft separation distance. Second, using state-space methods, a full-state feedback control is designed to control the combined attitude and separation distance. Full-state feedback control could be used for tighter mission requirements.

1. *Charge Feedback Control*

To stabilize the formation shape at the libration points, a similar active charge feedback law, introduced in [9] for the study of the linear dynamics of orbit radial two-craft formations at GEO, is applied at the libration point scenario. A proportional-derivative feedback control of δL is designed by defining [9]

$$\delta Q = \frac{m_1m_2L_{\text{ref}}^2}{(m_1+m_2)k_c}(-C_1\delta L - C_2\delta\dot{L}) \quad (24)$$

Substituting this expression for δQ in Eq. (23c), the closed-loop separation distance dynamics become

$$\delta\ddot{L} + (C_1 - 3(2\sigma+1)\Omega^2)\delta L + C_2\delta\dot{L} - (2\Omega L_{\text{ref}})\dot{\psi} = 0 \quad (25)$$

Because the δL differential equation does not involve a $\delta\dot{L}$ damping term, the derivative feedback is essential for asymptotic convergence. This charge feedback control law is implemented by determining the charges q_1 and q_2. Because $Q = q_1q_2$, using Eq. (22b), the spacecraft charges must satisfy

$$q_1 q_2 = Q_{\text{ref}} + \delta Q \tag{26}$$

where Q_{ref} value is evaluated from Eq. (21) while δQ value is given by the charge feedback law expression in Eq. (24). Due to the above constraint yielding an infinite number of solutions, the following implementation is used where equal charges in magnitude across the craft are chosen:

$$q_1 = \sqrt{|Q_{\text{ref}} + \delta Q|} \tag{27}$$

$$q_2 = -q_1 \tag{28}$$

Because $\delta Q \ll Q_{\text{ref}}$ and $Q_{\text{ref}} < 0$, note that here $Q_{\text{ref}} + \delta Q < 0$ which implies that $q_1 > 0$ and $q_2 < 0$.

To prevent numerical difficulties due to a small value of Ω, the linearized attitude dynamics Eqs. (23a, 23b) and the closed-loop separation distance dynamics given in Eq. (25) are made independent of Ω by the following transformation:

$$\mathrm{d}\tau = \Omega \, \mathrm{d}t \tag{29a}$$

$$(*)' = \frac{\mathrm{d}(*)}{\mathrm{d}\tau} = \frac{1}{\Omega}\frac{\mathrm{d}(*)}{\mathrm{d}t} \tag{29b}$$

Thus, the orbit rate Ω independent linearized equations of motion for a two-craft Coulomb tether formation at any collinear libration point are given by

$$\theta'' + (1 + 3\sigma)\theta = 0 \tag{30a}$$

$$\psi'' + \frac{2}{L_{\text{ref}}}\delta L' + 3\sigma\psi = 0 \tag{30b}$$

$$\delta L'' + \tilde{C}_2 \delta L' - (2L_{\text{ref}})\psi' + (\tilde{C}_1 - 3(2\sigma + 1))\delta L = 0 \tag{30c}$$

where $\tilde{C}_2 = \frac{C_2}{\Omega}$ and $\tilde{C}_1 = \frac{C_1}{\Omega^2}$ are nondimensionalized feedback gains. Routh–Hurwitz stability criteria are used to finetune these gain values that satisfy the stability requirements. The characteristic equation for the coupled δL and ψ equation is

$$\lambda^4 + \tilde{C}_2\lambda^3 + (\tilde{C}_1 + 1 - 3\sigma)\lambda^2 + 3\sigma\tilde{C}_2\lambda + 3\sigma(\tilde{C}_1 - 6\sigma - 3) = 0 \tag{31}$$

Roots of Eq. (31) should have negative real parts for asymptotic stability. For all roots to have negative real parts, a Routh table construction allows one to determine the following necessary constraints on the gains $\tilde{C}_1$ and $\tilde{C}_2$

$$\tilde{C}_1 > 6\sigma + 3 \tag{32a}$$

$$\tilde{C}_2 > \sqrt{n - 3(2\sigma + 1)} \tag{32b}$$

To fix the gain values that satisfy the stability criteria in Eq. (32), near-ideal damping conditions are assumed. Let the scaling factors n and β be positive and real such that the gains are rewritten as

$$\tilde{C}_1 = n > 6\sigma + 3 \tag{33a}$$

$$\tilde{C}_2 = \beta\sqrt{n - 3(2\sigma + 1)} \tag{33b}$$

The natural frequency of the ψ equation is $\sqrt{3\sigma}$ and is independent of the choice of $\tilde{C}_1$ and $\tilde{C}_2$, and the natural frequency for the δL equation is $\sqrt{n - 3(2\sigma + 1)}$. For the ψ' coupling term in the δL equation to serve as a defacto damping term, a value of $n = 9\sigma + 3$ will match these frequencies. Also, critical damping for the δL equation without the ψ' term is ensured for $\beta = 2$. Therefore, with the inclusion of the ψ' term for effective damping, one expects the value of n and β to be in the vicinity of $n = 9\sigma + 3$ and $\beta = 2$. At L_2 where $\sigma = 3.190432478$, the root locus plots for the coupled equations where the parameters are varied, $n = 26$ ensures good rates of convergence for all the modes and $\beta = 2.22$ satisfies effective damping for the modes. The optimal root locus plot is shown in Fig. 3.

2. *Application of Linear Quadratic Regulator Design*

To investigate the stability and control using the state feedback controller, a two-craft Coulomb tether formation at a collinear libration point must be represented in the following state-space form:

$$\dot{\boldsymbol{x}} = \boldsymbol{A}\boldsymbol{x} + \boldsymbol{B}\boldsymbol{u} \tag{34}$$

$$\boldsymbol{y} = \boldsymbol{C}\boldsymbol{x} \tag{35}$$

where the state $\boldsymbol{x}$ is

$$\boldsymbol{x} = [\theta, \dot{\theta}, \psi, \dot{\psi}, \delta L, \dot{\delta L}]^T \tag{36}$$

Using the Coulomb control as an actuator mechanism, the $\boldsymbol{A}$ and $\boldsymbol{B}$ matrices can be represented from Eqs. (23a–23c). As previously seen, the out-of-plane $\theta(t)$ motion is decoupled from the in-plane motion ($\psi(t)$ and $\delta L(t)$), which can be formally examined by checking the *controllability* of the system [17]. Because the rank of the controllability matrix is 4 and the number of state variables is 6, the tether formation is not completely controllable with charge only. When the out-of-plane $\theta(t)$ motion is not considered, then, with the reduced state space of four state variables $\boldsymbol{x} = [\psi, \dot{\psi}, \delta L, \dot{\delta L}]^T$, the rank of the controllability matrix is 4. Therefore, subsequent analysis uses the following reduced $\boldsymbol{A}$ and $\boldsymbol{B}$ matrices

$$\boldsymbol{A} = \begin{bmatrix} 0 & 1 & 0 & 0 \\ -3\sigma & 0 & 0 & -\dfrac{2}{L_{\text{ref}}} \\ 0 & 0 & 0 & 1 \\ 0 & 2L_{\text{ref}} & 3(2\sigma + 1) & 0 \end{bmatrix} \tag{37}$$

$$\boldsymbol{B} = \begin{bmatrix} 0 & 0 & 0 & \dfrac{k_c}{m_1}\dfrac{1}{L_{\text{ref}}^2}\dfrac{m_1 + m_2}{m_2} \end{bmatrix}^T \tag{38}$$

If only the length and length rate state variables are available from the measurements of an optical sensor, then the remaining two state variables (pitch and pitch rate) must be estimated from the output measurements. Therefore, the $\boldsymbol{C}$ matrix in the output equation becomes

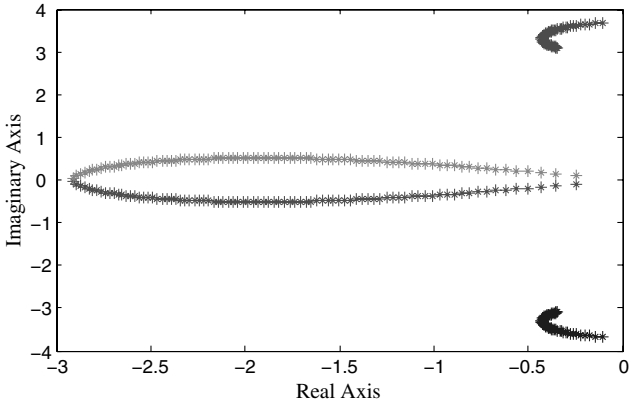

Fig. 3 Root locus plot of the linearized differential equations at L_2 for gain $\beta = 2.22$.

$$\boldsymbol{C} = \begin{bmatrix} 0 & 0 & 1 & 0 \\ 0 & 0 & 0 & 1 \end{bmatrix} \tag{39}$$

However, the $\boldsymbol{C}$ matrix should satisfy the *observability* condition [17]. Because the rank of the observability matrix is 4, the values of the ψ and $\dot{\psi}$ states can be estimated from the measured outputs δL and $\dot{\delta L}$. Also, the observability of the angles using δL and $\dot{\delta L}$ is only possible in the absence of differential solar radiation pressure on the formation. Hence, the in-plane linear model of a two-craft Coulomb tether formation at a collinear libration point is both controllable and observable.

Assuming that the information about all four state variables is available either through direct measurement or by estimation, the following feedback control is used to control the system with the feedback gain matrix $\boldsymbol{K}$, computed using either the pole placement method or the linear quadratic regulator (LQR) method

$$\boldsymbol{u} = -\boldsymbol{K}\boldsymbol{x} \tag{40}$$

Here the LQR methodology is applied to determine the optimal control $\boldsymbol{u}$ such that the gain vector $\boldsymbol{K}$ minimizes the performance index

$$J = \int_0^\infty (\boldsymbol{x}^T \boldsymbol{W}_Q \boldsymbol{x} + \boldsymbol{u}^T \boldsymbol{W}_R \boldsymbol{u})\, \mathrm{d}T \tag{41}$$

where $\boldsymbol{W}_Q$ and $\boldsymbol{W}_R$ are the weighting matrices that are used as design parameters. One can establish a faster response for in-plane control by selecting appropriate weighting matrices for which the settling time is less than one orbit.

C. Numerical Simulation

The performance and stability of a 25 m Coulomb virtual tether formation is illustrated in the following numerical simulation. Table 1 lists the simulation parameters and the values used. The parameters n and β are selected based on root locus plot analysis where the gains $\tilde{C}_1$ and $\tilde{C}_2$ computed from Eq. (33) satisfy the stability critera in Eq. (32) and also lead to effective damping. The two-craft Coulomb tether performance at the collinear libration point L_2 is simulated by integrating the linearized equations of motion in Eq. (30) and then compared with the results obtained from integrating the nonlinear equations of motion in Eq. (18). During this simulation, the debye length is assumed to be zero to investigate the effects of linearization on the relative motion.

Figure 4a shows the Coulomb tether motion with the proportional-derivative charge feedback law in Eq. (24). Both the yaw motion ψ and the separation distance deviation δL converged to zero. Therefore, stabilizing the separation distance to zero also stabilized the in-plane rotation angle after about 1.3 orbits, and the uncoupled roll motion θ is a stable sinusoidal motion as expected. Furthermore, Fig. 4a shows that the nonlinear simulation shown as dashed lines closely follows the linearized simulation. Whereas the δL states asymptotically converge to zero in the linearized simulation, they reach steady-state oscillations in the nonlinear simulation. This notable difference is observed in the two-body system as well [9]. Using the same reference charge product Q_{ref} computated from Eq. (24) for both simulations resulted in this inconsistent behavior. This charge yields a static formation in the linearized formulation; however, in the nonlinear formulation, this charge will not yield a static formation. This is due to the charge feedback control not operating about a steady-state charge in the nonlinear problem. Although the δL and ψ errors converge to zero in the nonlinear simulation, the discrepancies in charge computation between the linear and nonlinear simulations cause the orbital dynamics to perturb the system [9]. This makes the states grow again, resulting in these steady-state oscillations. Therefore, for the nonlinear problem, a control strategy could be implemented wherein the Q_{ref} value could be numerically recomputed. Despite this deviation, the nonlinear and linear simulation results compare very well, thus validating the performance prediction of the linearized analysis.

Table 1 Input parameters used in the simulation for L_2

Parameter	Value	Units
m_1	150	kg
m_2	150	kg
L_{ref}	25	m
k_c	8.99×10^9	$\frac{\text{Nm}^2}{\text{C}^2}$
Q_{ref}	−0.006816	μC^2
Ω	2.661699×10^{-6}	rad/s
$\delta L(0)$	0.5	m
$\varphi(0)$	0.1	rad
$\theta(0)$	0.1	rad
n	26	
β	2.22	
σ	3.190432478	

Figure 4b shows the spacecraft control charge q_1 usage for both the linear and nonlinear simulation formulations. The charge results for both converge to the static equilibrium reference value q_{1r}. For orbit-radial equilibrium, the control charge q_1 is the negative of q_2. Because the control charges are on the order of micro-Coulombs, they can easily be implemented in practice using charge emission devices.

A numerical simulation using an optimal regulator results in a settling time of less than one orbit, a maximum overshoot of less than ± 2.5 m in separation distance and $\pm .1$ rad in pitch angle variation. A faster response for in-plane control than that of a charge feedback control law can be obtained by selecting appropriate $\boldsymbol{W_Q}$ and $\boldsymbol{W_R}$ weighting matrices. The following $\boldsymbol{W_Q}$ and $\boldsymbol{W_R}$ matrices allow the settling time to be less than one orbit

$$\boldsymbol{W_Q} = \begin{bmatrix} 75 & 0 & 0 & 0 \\ 0 & 0.0001 & 0 & 0 \\ 0 & 0 & 0.1 & 0 \\ 0 & 0 & 0 & 0.000001 \end{bmatrix} \quad \text{and} \quad \boldsymbol{W_R} = 10,000 \tag{42}$$

Figure 5 shows the state response of the system for the LQR method. The results indicate that with the acceptable limits for separation distance and attitude variations, the settling time is around one orbit. However, the maximum overshoot increases the charge requirements as compared with using the charge feedback law in Eq. (24). For subsequent analysis, we use the charge control law because of the minimal number of control variables used in it.

III. Linear Dynamics and Stability Analysis—Trianglular Libration Points

A. Charged Relative Equations of Motion

This section derives the equations of motion of a two-craft Coulomb tether whose center of mass is at the triangular equilibrium point L_4 as shown in Fig. 6 and nominally aligned in the orbit-radial direction of the orbit frame. This derivation closely resembles the derivation of the equations of motion for a two-craft Coulomb tether at any collinear libration point given in Sec. II. The two distance vectors $\boldsymbol{R}_1$ and $\boldsymbol{R}_2$ of L_4 in the synodic frame from the two primaries in the plane are given by

$${}^{\mathcal{S}}\boldsymbol{R}_1 = \begin{bmatrix} r_{x_0} + d_1 \\ r_{y_0} \\ 0 \end{bmatrix} \quad \text{and} \quad {}^{\mathcal{S}}R_2 = \begin{bmatrix} r_{x_0} - d_2 \\ r_{y_0} \\ 0 \end{bmatrix} \tag{43}$$

The expressions for the kinetic energy in Eq. (10) and Coulomb potential in Eq. (16) remain the same. However, the gravitational potential in Eq. (15) involves adding the two position vectors $\boldsymbol{R}_i + \boldsymbol{\rho}_i$, where $\boldsymbol{R}_i$ is in the synodic frame $\mathcal{S}$ and $\boldsymbol{\rho}_i$ is in the orbiting frame $\mathcal{O}$. Therefore, the vectors $\boldsymbol{R}_i$ are expressed in its orbiting frame components using the transformation ${}^{\mathcal{O}}\boldsymbol{R}_i = [OS]^{\mathcal{S}}\boldsymbol{R}_i$ with the transformation matrix $[OS]$ given by

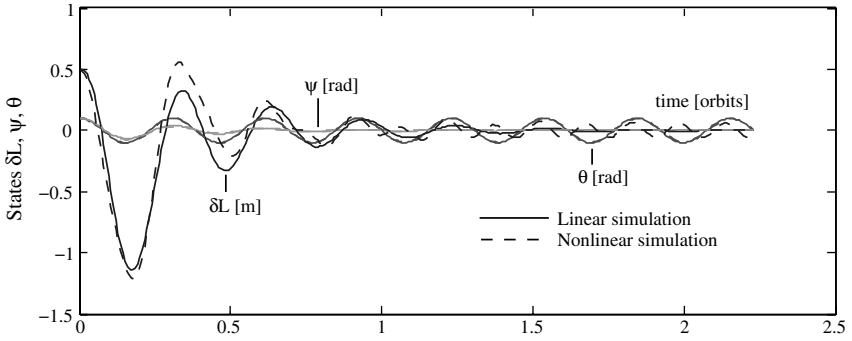

a) Time histories of length variations δL, in-plane pitch angle ψ, and out-of-plane roll angle θ

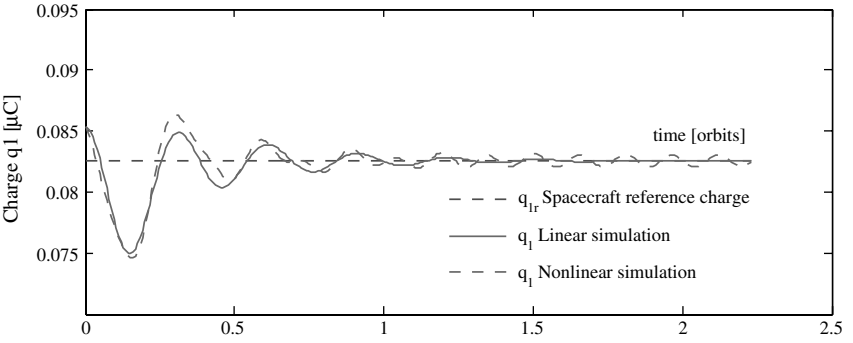

b) Spacecraft charge time histories

Fig. 4 Simulation results from integrating the linearized and nonlinear equations of motion at L_2.

$$[OS] = \begin{bmatrix} \cos\alpha & \sin\alpha & 0 \\ -\sin\alpha & \cos\alpha & 0 \\ 0 & 0 & 1 \end{bmatrix} \tag{44}$$

where α is the angle between the synodic frame at the barycenter O and the orbiting frame at L_4 as shown in Fig. 6. For the Earth–moon system, the value of α is 60.31 deg [11].

Using the Lagrangian formulation in Eq. (17), the nonlinear equations governing the roll angle θ out of the orbital plane, the pitch angle ψ in the orbital plane, and the separation distance L thus obtained are

$$\ddot{\theta} + \frac{2\dot{L}}{L}\dot{\theta} + \cos\theta\sin\theta((\dot{\psi}+\Omega)^2 + \frac{3\Omega^2}{4}((1-\nu)(A_\alpha\cos\psi + B_\alpha\sin\psi)^2 + \nu(C_\alpha\cos\psi + D_\alpha\sin\psi)^2)) = 0 \tag{45a}$$

$$\ddot{\psi} - 2\dot{\theta}\tan\theta(\dot{\psi}+\Omega) + \frac{2\dot{L}}{L}(\dot{\psi}+\Omega) - \frac{3}{4}\Omega^2 \times \left((1-\nu)\left(A_\alpha B_\alpha\cos 2\psi + \frac{B_\alpha^2 - A_\alpha^2}{2}\sin 2\psi\right) + \nu\left(C_\alpha D_\alpha\cos 2\psi + \frac{D_\alpha^2 - C_\alpha^2}{2}\sin 2\psi\right)\right) = 0 \tag{45b}$$

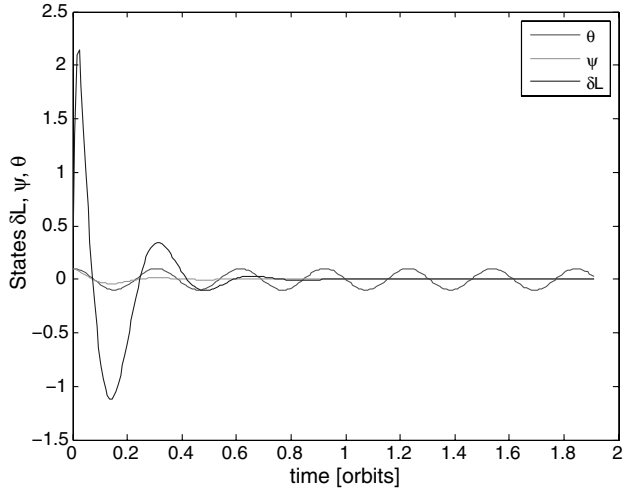

Fig. 5 LQR time histories of length variations δL, pitch angle ψ, and roll angle θ.

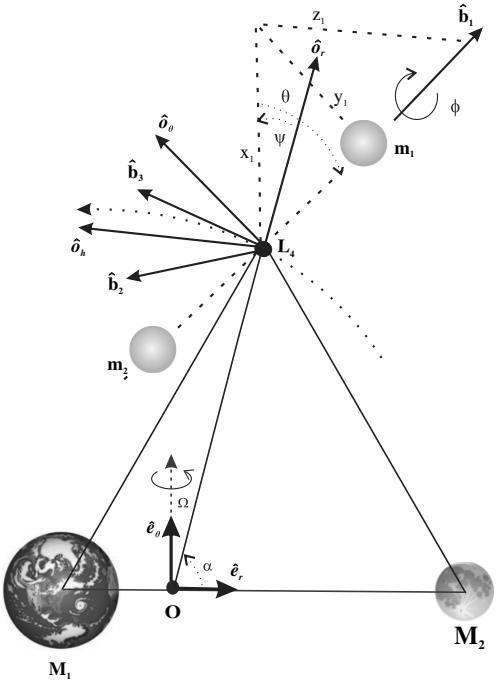

Fig. 6 Euler angles representing the attitude of Coulomb tether with respect to the orbit frame at L_4.

$$\ddot{L} - L(\dot{\theta}^2 + (\dot{\psi} + \Omega)^2\cos^2\theta - \Omega^2) + \frac{3}{4}L\Omega^2\cos^2\theta((1-\nu)(A_\alpha\cos\psi + B_\alpha\sin\psi)^2 + \nu(C_\alpha\cos\psi + D_\alpha\sin\psi)^2) - k_c\frac{m_1+m_2}{m_1m_2}q_1q_2e^{-L/\lambda d}\left(\frac{L+\lambda_d}{L^2\lambda_d}\right) = 0 \tag{45c}$$

where

$$A_\alpha = \cos\alpha + \sqrt{3}\sin\alpha \tag{46a}$$

$$B_\alpha = -\sin\alpha + \sqrt{3}\cos\alpha \tag{46b}$$

$$C_\alpha = -\cos\alpha + \sqrt{3}\sin\alpha \tag{46c}$$

$$D_\alpha = \sin\alpha + \sqrt{3}\cos\alpha \tag{46d}$$

The linearized version of the nonlinear equations in Eq. (45) comes from expanding in a Taylor series about the equilibrium states given in Eq. (20). Both the roll and pitch equations of motion are linearized about small roll and pitch angles, respectively. The separation distance equations of motion are linearized about small variations in δL as well as small variations in the product charge term δQ defined as in Eq. (22). Mission requirements determine the reference separation length L_{ref}, and Q_{ref} is determined from the following constraint on a particular choice of L_{ref}

$$Q_{\text{ref}} = -\frac{3}{4}\sigma_{EQRE1}\Omega^2\frac{L_{\text{ref}}^3}{k_c}\frac{m_1m_2}{m_1+m_2} \tag{47}$$

where

$$\sigma_{EQRE1} = 1 + 2\sin^2\alpha + \sqrt{3}\sin 2\alpha(1-2\nu) \tag{48}$$

Performing the necessary linearizations yields

$$\ddot{\theta} + \left(1 + \frac{3}{4}\sigma_{EQRE1}\right)\Omega^2\theta = 0 \tag{49a}$$

$$\ddot{\psi} + \frac{2\Omega}{L_{\text{ref}}}\delta\dot{L} - \frac{3}{2}\sigma_{EQRE3}\Omega^2\psi = 0 \tag{49b}$$

$$\delta\ddot{L} - 2\Omega L_{\text{ref}}\dot{\psi} - \frac{9}{4}\sigma_{EQRE1}\Omega^2\delta L - \frac{3}{2}L_{\text{ref}}\sigma_{EQRE2}\Omega^2\psi - \left(\frac{k_c}{m_1}\frac{1}{L_{\text{ref}}^2}\frac{m_1+m_2}{m_2}\right)\delta Q = 0 \tag{49c}$$

with

$$\sigma_{EQRE2} = \sqrt{3}\cos 2\alpha(1-2\nu) + \sin 2\alpha \tag{50}$$

$$\sigma_{EQRE3} = \sqrt{3}\sin 2\alpha(2\nu-1) + \cos 2\alpha \tag{51}$$

Thus, Eqs. (49a) and (49b) represent the linearized attitude dynamics of the Coulomb tether body frame $\mathcal{B}$ and Eq. (49c) represents the linearized separation distance differential equation about the static nadir reference configuration at a triangular libration point. As opposed to the collinear solution, the ψ term here is a new component; however, due to the quite small value of $\sigma_{EQRE2} = -2.0405 \times 10^{-4}$ at L_4, its effect is negligible on the separation distance differential equation. Furthermore, because $\sigma_{EQRE1} = 3.963662$ and $\sigma_{EQRE3} = -1.963662$, the dynamics at L_4 become very similar to those found in [9] for an orbit radial two-craft formation at GEO. Hence, the stability behavior should be approximately the same as that observed in [9].

B. Charge Feedback Control

Using the proportional-derivative feedback control of δL from Eq. (24), the orbit rate Ω independent linearized equations of motion for a two-craft Coulomb tether formation at the triangular libration point L_4 are given by

$$\theta'' + \left(1 + \frac{3}{4}\sigma_{EQRE1}\right)\theta = 0 \tag{52a}$$

$$\psi'' + \frac{2}{L_{\text{ref}}}\delta L' - \frac{3}{2}\sigma_{EQRE3}\psi = 0 \tag{52b}$$

$$\delta L'' + \tilde{C}_2\delta L' - (2L_{\text{ref}})\psi' - \left(\frac{3}{2}L_{\text{ref}}\sigma_{EQRE2}\right)\psi - \left(\frac{9}{4}\sigma_{EQRE1} - \tilde{C}_1\right)\delta L = 0 \tag{52c}$$

where $\tilde{C}_2 = \frac{C_2}{\Omega}$ and $\tilde{C}_1 = \frac{C_1}{\Omega^2}$ are nondimensionalized feedback gains. Routh–Hurwitz stability critera can be used to finetune these gain values that satisfy the stability requirements. The characteristic equation for the coupled δL and ψ equation is

$$\lambda^4 + \tilde{C}_2\lambda^3 + \left(\tilde{C}_1 + 4 - \frac{3}{2}\sigma_{EQRE3} - \frac{9}{4}\sigma_{EQRE1}\right)\lambda^2 + \left(3\sigma_{EQRE2} - \frac{3}{2}\sigma_{EQRE3}\tilde{C}_2\right)\lambda + \tfrac{3}{2}\sigma_{EQRE3}\left(\tfrac{9}{4}\sigma_{EQRE1} - \tilde{C}_1\right) = 0 \tag{53}$$

Roots of this equation should have negative real parts for asymptotic stability. A Routh table allows one to determine the following necessary constraints on the gains $\tilde{C}_1$ and $\tilde{C}_2$ that ensures all roots have negative real parts

$$\tilde{C}_1 > \frac{9}{4}\sigma_{EQRE1} \tag{54a}$$

$$\tilde{C}_2 > 0 \tag{54b}$$

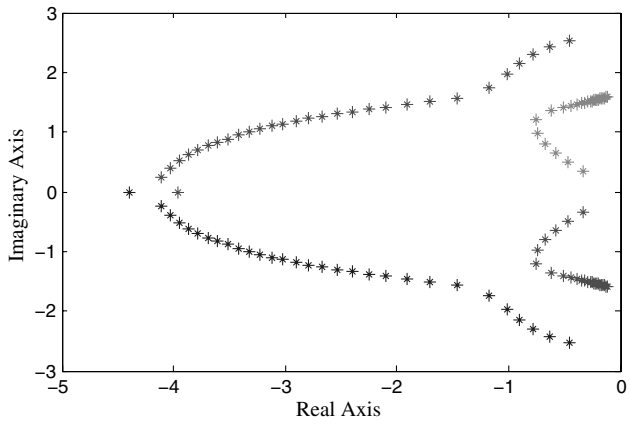

Fig. 7 Root locus plot of the linearized differential equations at L_4 for gain $\beta = 2.22$.

Table 2 Input parameters used in the simulation for L_4

Parameter	Value	Units
Q_{ref}	−0.002745	μC^2
n	11.71	
β	2.22	
σ_{EQRE1}	3.963662	
σ_{EQRE2}	-2.0405×10^{-4}	
σ_{EQRE3}	−1.963662	

To fix the gain values that satisfy the stability critera in Eq. (54), near-ideal damping conditions are assumed. Let the scaling factors n and β be positive and real, allowing the gains to be rewritten as

$$\tilde{C}_1 = n > \frac{9}{4}\sigma_{EQRE1} \tag{55a}$$

$$\tilde{C}_2 = \beta\sqrt{n - \frac{9}{4}\sigma_{EQRE1}} \tag{55b}$$

Following the same line of reasoning discussed for collinear libration points earlier and studying the root locus plots for the coupled equations where the n and β parameters are varied, $n = 11.71$ ensures good rates of convergence for all the modes and $\beta = 2.22$ provides effective damping for the modes. The optimal root locus plot is shown in Fig. 7.

C. Numerical Simulation

Except for the parameters listed in Table 2, the remaining simulation parameter values used are shown in Table 1. The parameter $n = 11.71$ for L_4 is obtained from the root locus plot analysis. The gains $\tilde{C}_1$ and $\tilde{C}_2$ computed from Eq. (55) satisfy the stability critera in Eq. (54) and also yield effective damping. Integrating the linearized equations of motion in Eq. (52) simulates the two-craft Coulomb tether performance at L_4. This is then compared with the results obtained from integrating the nonlinear equations of motion in Eq. (45). Figure 8a illustrates the Coulomb tether motion with the proportional-derivative charge feedback law. Both the yaw motion ψ and the separation distance deviation δL converge to zero. Therefore, stabilizing the separation distance to zero also stabilized the in-plane rotation angle after about one orbit, and the uncoupled roll motion θ is a stable sinusoid as expected. Furthermore, Fig. 8a shows that the nonlinear simulation plotted as dashed lines closely follows the linearized simulation; whereas the δL states asymptotically converge to zero in the linearized simulation, they reach steady-state oscillations in the nonlinear simulation. The reasons for this notable difference are already explained in numerical simulation part of Sec. II. Despite this difference, the nonlinear and linear simulation results compare very well, thus justifying the linearization assumptions used. Figure 8b shows the spacecraft control charge q_1 usage for both linear and nonlinear simulation formulations. The charge results for both converge to the static equilibrium reference value q_{1r}. The control charges required for L_4 are less than those of L_2, which are on the order of micro-Coulombs and can easily be implemented in practice using charge emission devices.

IV. Conclusions

The feasibility of a two-craft Coulomb tether concept is studied at libration points for orbit-radial equilibrium. The new two-craft dynamics at the libration points is provided as a general framework in which circular Earth orbit dynamics form a special case. Although the orbit-radial dynamics at libration points are slightly different than of those found in [9] for an orbit radial two-craft formation at geostationary orbit, the stability conditions are similar. At libration points, the out-of-plane motion is marginally stable and decoupled from the in-plane motion. The in-plane motion is stabilized using only separation distance measurements (computing rates). A linearized charge feedback law stabilizes the separation distance using Coulomb force and exploits the gravity gradient torque due to the two primaries to stabilize the in-plane attitude motion. Also, a full-state feedback linear quadratic regulator meets variable mission requirements (i.e., stabilizing the formation within a given time). The

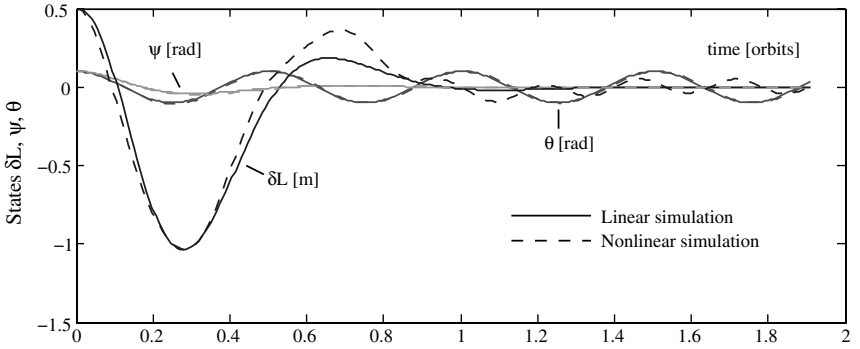

a) Time histories of length variations δL, in-plane pitch angle ψ, and out-of-plane roll angle θ

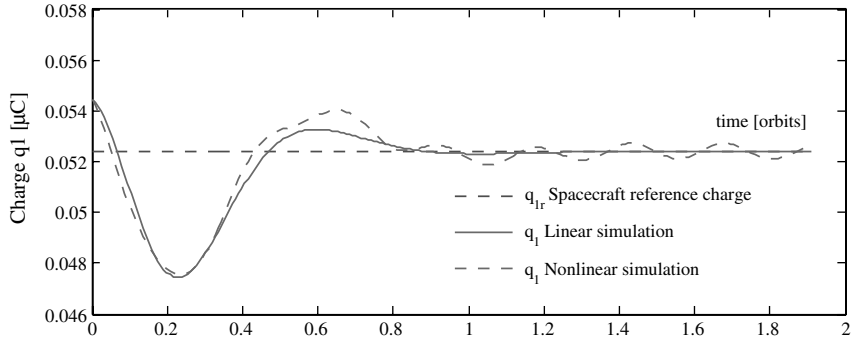

b) Spacecraft charge time histories

Fig. 8 Simulation results from integrating the linearized and nonlinear equations of motion at L_4.

linearized feedback laws assume that the differential solar radiation pressure on the formation is zero. Numerical simulations at L_2 and L_4 with the charge feedback law show that the formation stabilized faster at L_4 (within one orbit) than at L_2 (1.3 orbits). This is perhaps due to the unstable nature of the collinear libration point causing a slow stabilization of the formation. Also, due to the smaller rotation rate of the Earth–moon barycenter, the micro-Coulomb charge requirements at the libration points is at least an order of magnitude smaller compared with that of a two-body system in [9].

References

[1] King, L. B., Parker, G. G., Deshmukh, S., and Chong, J. -H., "Spacecraft Formation-Flying Using Inter-Vehicle Coulomb Forces," NASA TR, Jan. 2002

[2] King, L. B., Parker, G. G., Deshmukh, S., and Chong, J. -H., "Study of Interspacecraft Coulomb Forces and Implications for Formation Flying," *Journal of Propulsion and Power*, Vol. 19, No. 3, 2003, pp. 497–505. doi:10.2514/2.6133

[3] Cover, J. H., Knauer, W., and Maurer, H. A., Lightweight Reflecting Structures Utilizing Electrostatic Inflation, U.S. Patent 3,546,706, Oct. 1966.

[4] Berryman, J., and Schaub, H., "Analytical Charge Analysis for 2- and 3-Craft Coulomb Formations," *Journal of Guidance, Control, and Dynamics*, Vol. 30, No. 6, 2007, pp. 1701–1710. doi:10.2514/1.23785

[5] Vasavada, H., and Schaub, H., "Analytic Solutions for Equal Mass 4-Craft Static Coulomb Formation," *Journal of Astronautical Sciences*, Vol. 56, No. 1, Jan.–March 2008, pp. 7–40.

[6] Berryman, J., and Schaub, H., "Static Equilibrium Configurations in GEO Coulomb Spacecraft Formations," *AAS/AIAA Space Flight Mechanics Meeting*, AIAA Paper 2005-104, 2005.

[7] Schaub, H., Hall, C. D., and Berryman, J., "Necessary Conditions for Circularly-Restricted Static Coulomb Formations," *Journal of Astronautical Sciences*, Vol. 54, Nos. 3–4, July–Dec. 2006, pp. 525–541.

[8] Beck, J. A., "Relative Equilibria of a Rigid Satellite in a Central Gravitational Field," Ph.D. Thesis, AFIT/DS/ENY/97-6, U.S. Air Force Inst. of Technology, Wright–Patterson AFB, OH, Sept. 1997.

[9] Natarajan, A., "A Study of Dynamics and Stability of Two-Craft Coulomb Tether Formations," Ph.D. Dissertation, Aerospace and Ocean Engineering Dept., Virginia Polytechnic Inst. and State Univ., Blacksburg, VA, May 2007.

[10] Inampudi, R., and Schaub, H., "Two-Craft Coulomb Formation Relative Equilibria about Circular Orbits and Libration Points," *AAS/AIAA Space Flight Mechanics Meeting*, AAS Paper 10-163, 2010.

[11] Misra, A. K., Bellerose, J., and Modi, V. J., "Dynamics of a Tethered System near the Earth–Moon Lagrangian Points," *Proceedings of the 2001, AAS/AIAA Astrodynamics Specialist Conference*, Vol. 109, Advances in the Astronautical Sciences, Quebec City, Canada, 2002, pp. 415–435.

[12] Pettazzi, L., Krüger, H., Theil, S., and Izzo, D., "Electrostatic Forces for Satellite Swarm Navigation and Reconfiguration," ESA TR ARI-SS-FP-ZAR-001, 2006.

[13] Schaub, H., and Junkins, J. L., "Particle Kinematics," *Analytical Mechanics of Space Systems*, AIAA, Reston, VA, 2003, pp. 11–13.

[14] Romanelli, C. C., Natarajan, A., Schaub, H., Parker, G. G., and King, L. B., "Coulomb Spacecraft Voltage Study Due to Differential Orbital Perturbations," *AAS/AIAA Space Flight Mechanics Meeting*, AAS Paper 06-123, 2006.

[15] Hastings, D., and Garrett, H., "Plasma Interactions," *Spacecraft-Environment Interactions*, Cambridge Univ. Press, Cambridge, England, U.K., 2004, pp. 147–206.

[16] Murdoch, N., Izzo, D., Bombardelli, C., Carnelli, I., Hilgers, A., and Rodgers, D., "The Electrostatic Tractor for Asteroid Deflection," *58th International Astronautical Congress*, Paper IAC-08-A3.I.5, 2008.

[17] Brogan, W. L., "Controllability and Observability for Linear Systems," *Modern Control Theory*, 3rd ed., Prentice–Hall, Upper Saddle River, NJ, 1990, pp. 373–379.